2-4 Interplanetary Magnetic Flux Ropes

MARUBASHI Katsuhide

The purpose of this review is to examine the possibility of predicting large geomagnetic storms from solar observations. We focus on three topics: (1) the relationship between coronal magnetic fields and interplanetary magnetic flux ropes, (2) the role of magnetic flux ropes in geomagnetic storms, and (3) further studies needed for improving our ability to predict geomagnetic storms based on our knowledge of interplanetary magnetic flux ropes. Evidence is presented that the magnetic structures of magnetic flux ropes are strongly controlled by large-scale magnetic fields in the solar source regions of coronal mass ejections. The relationship suggests the possibility of predicting the variations in interplanetary magnetic fields based on solar observations at the time of launch of coronal mass ejections. An analysis of one particular geomagnetic storm reveals the necessity of further precise knowledge on the global topology of flux ropes in interplanetary space. Finally, we suggest some important problems to be studied in the future.

Keywords
Solar wind, Interplanetary magnetic field, Interplanetary magnetic flux rope, Coronal mass ejection, Solar magnetic field, Filament disappearance

1 Introduction

Space weather is defined as conditions in electromagnetic fields and the plasma and radiation environment in space surrounding the earth, including the ionosphere and the upper atmosphere[1]. A geomagnetic storm is one of the two main phenomena significantly affecting space weather, the other being explosive solar activities such as solar flares and coronal mass ejections (CME). Solar wind disturbances supply energy to the magnetosphere and create geomagnetic storms that greatly alter the internal conditions of the Earth's space environment, from the entire magnetosphere all the way to the ionosphere and the upper atmosphere. There are several known types of solar wind disturbances that cause geomagnetic storms[2]. Among them, plasma masses ejected from the solar corona during CMEs are known as main causes of major geomagnetic storms. These plasma masses are sometimes called plasma clouds occurring in interplanetary space.

Numerous attempts have been made to identify plasma and magnetic field characteristics specific to CME-generated plasma clouds based on solar wind observation data. This has been a major theme in the study of solar wind disturbances since the early days of solar wind observations[3][4]. The three most widely observed characteristics of plasma clouds are (1) the bi-directional hot electron flux[5], (2) an abnormally low proton temperature[6], and (3) twists in the magnetic field lines referred to as "magnetic flux ropes"[7]. The interplanetary magnetic flux rope, the main subject of this paper, is found in a CME-generated plasma cloud as a part of structure with a rope-like magnetic feature.

The interplanetary magnetic field (IMF) plays an important role in energy transfer from the solar wind to the magnetosphere. The energy transfer is most effective during strong southward IMF[8]. Interplanetary magnetic flux ropes often contain strong southward IMF, which generate large geomagnetic storms. When a shock is created in front of the flux rope, a strong southward IMF is produced in the shocked solar wind, which also contributes to geomagnetic storm development. Thus, the interplanetary magnetic flux rope is an important factor in geomagnetic storm development. On the other hand, it has been pointed out that the interplanetary magnetic flux rope carries magnetic fields from the source region of CME retaining its original structure to a certain extent[9]-[12]. These facts suggest that the structure of the CME source region is an important determinant of the structure of interplanetary magnetic flux ropes; this structure controls geomagnetic storm development. Thus, we can see a possibility that the study of interplanetary magnetic flux ropes can lead to the prediction of geomagnetic storms in the future.

The purpose of this paper is to explain how the study of interplanetary magnetic flux ropes can pave the way for the prediction of geomagnetic storms. Section 2 will first describe a method of analysis to determine the shape of the interplanetary magnetic flux rope, and then will examine the relationship between the obtained interplanetary magnetic flux rope structure and the magnetic field structure of the CME source region. Section 3 will give a concise description of a geomagnetic storm triggered by an interplanetary magnetic flux rope. Finally, Section 4 will discuss future research themes required to further clarify the relationship between CME-generated plasma clouds and magnetic flux ropes.

2 Interplanetary Magnetic Flux Ropes and CMEs

Magnetic field structures referred to as magnetic flux ropes have been studied in connection with filamentary inhomogeneity often observed in low density plasma in space[13]. Burlaga's group[14] was the first to find a peculiar magnetic field structure in a plasma cloud, which they named "magnetic cloud." However, it was only through successive analyses that an explanation was provided for the observed changes in the magnetic field based on the concept of magnetic flux ropes[15][7]. Later, a number of revisions were made to the interplanetary magnetic flux rope model[16][17], and more advanced methods of analysis have also been developed[18][10]. Results of such studies have shown that the generation of interplanetary magnetic flux ropes is closely connected to CME generation.

2.1 Magnetic Flux Ropes

A plasma in static equilibrium with no external forces acting on it satisfies the following equation.

$$-\nabla p+\vec{J}\times\vec{B}=0 \tag{1}$$

Here, P is plasma pressure, $\vec{J}$ is electric current density, and $\vec{B}$ is magnetic flux density.

When plasma is sufficiently rarefied and plasma pressure is low enough to be negligible, a state is realized in which the electromagnetic force of the second term is also zero. In other words, within plasma with a magnetic field, the electric current can only flow in the direction parallel or anti-parallel to the magnetic field. Such a magnetic field configuration is referred to as a "force-free field." Since $\vec{J}=rot\vec{B}/\mu_0$, the condition for the electric current to be parallel to the magnetic field is:

$$rot\vec{B}=\alpha\vec{B}\ (\alpha>0) \tag{2}$$

and

$$(\nabla\alpha)\cdot\vec{B}=0 \tag{3}$$

Let us consider the simplest case where α is a constant. It is referred to as a "force-free field with constant α." When axial symmetry is assumed, the above condition is expressed using the r, φ, and z components of a cylindrical coordinate.

$$-\frac{dB_z}{dr}=\alpha B_\varphi \tag{4}$$

$$\frac{1}{r}\frac{d}{dr}\left(rB_\varphi\right)=\alpha B_z \tag{5}$$

By eliminating B_φ , we obtain:

$$\left[\frac{d^2}{dr^2}+\frac{1}{r}\frac{d}{dr}+\alpha^2\right]B_z=0 \quad (6)$$

The solution for this equation is given by the 0-th order Bessel function:

$$B_z = AJ_0(\alpha r) \quad (7)$$

Here, A is an arbitrary constant. From Eq. (4),

$$B_\varphi = AJ_1(\alpha r) \quad (8)$$

For the case of electric current anti-parallel to the magnetic field, we start from:

$$rot\vec{B} = -\alpha\vec{B}\ (\alpha > 0) \quad (9)$$

and, in a similar manner, obtain:

$$B_z = AJ_0(\alpha r) \quad (10)$$

$$B_\varphi = -AJ_1(\alpha r) \quad (11)$$

Fig.1 is a schematic diagram showing internal magnetic fields in an axially symmetric, cylindrical structure with parallel and anti-parallel electric currents. Note that the axial magnetic flux density is assumed to be B_0, and that a surface where the axial magnetic field strength is 0 is taken as the external boundary. It can be easily seen from the magnetic field configurations how the magnetic flux rope acquired its name. The magnetic flux rope given by Eqs. (7) and (8) is referred to as the "parallel" type, in accordance with the direction of electric current parallel to the magnetic field. Conversely, the magnetic flux rope given by Eqs. (10) and (11) is referred to as the "anti-parallel" type. These are also referred to as "right-handed" and "left-handed" types based on the twist direction of the magnetic field lines. Fig.2 shows the change in the magnitude of B_z and B_φ with distance from axis.

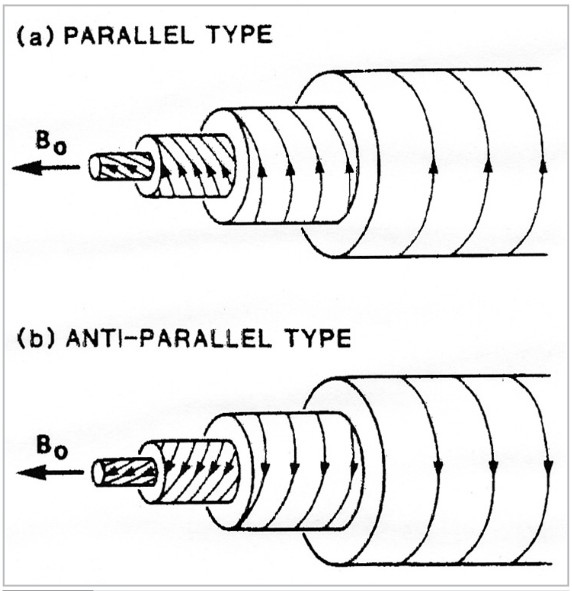

Fig.1 Schematic diagram of the internal magnetic field of the magnetic flux rope

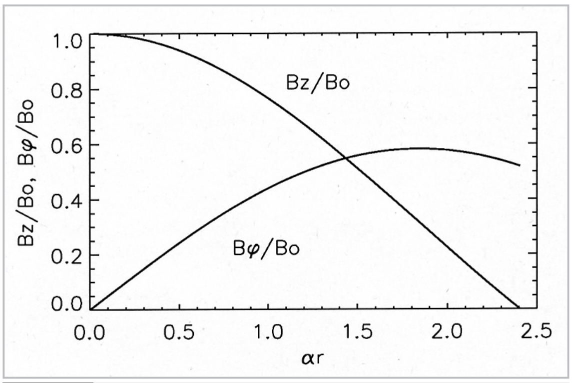

Fig.2 Change in B_z and B_φ as a function of distance from axis

2.2 Analysis of Magnetic Flux Ropes

The orientations and sizes of the observed magnetic flux ropes can be determined by fitting the observed changes in the solar wind magnetic fields to the flux rope model. This analysis is important when studying the generation of a magnetic flux rope and its interaction with the magnetosphere. We describe a non-linear least-squares fitting analysis[10] based on a self-similar expansion model of a cylindrical magnetic flux rope of constant-α force-free configuration[17].

If we assume that a satellite encounters a cylindrical magnetic flux rope with radius R_0 after the self-similar expansion for the time duration t_0, radius R and the radial expansion velocity $\vec{v}$ at time $t_0 + t$ can be expressed by the following equations using the cylindrical coordinates r, φ, and z[17].

$$R = R_0(1 + t/t_0) \quad (12)$$

$$\vec{v} = v_r \vec{e_r} \quad (13)$$

$$v_r = r/(t + t_0) \qquad (r \leq R) \quad (14)$$

The internal magnetic field structure of the magnetic flux ropes can be expressed as follows:

$$\vec{B} = B_\varphi \vec{e_\varphi} + B_z \vec{e_z} \quad (15)$$

$$B_\varphi = sB_0 J_1(\alpha r)/(1 + t/t_0) \quad (16)$$

$$B_z = B_0 J_0(\alpha r)/(1 + t/t_0)^2 \quad (17)$$

Here, B_0 is the magnetic flux density at the axis of the cylinder, with the z-axis coinciding with the direction of the magnetic field at the axis. The direction of the twist of magnetic field line is represented by the parameters, with $s = 1$ and $s = -1$ corresponding to parallel and anti-parallel magnetic flux rope types, respectively. The constant α is selected so that αR is the initial zero point of the Bessel function J_0.

To calculate the magnetic field and solar wind velocities that would be observed by a satellite crossing the magnetic flux rope given by the above equations, the orientation of the magnetic flux rope in space and the geometrical relationship to the trajectory of the satellite must be assumed. The orientation of the magnetic flux rope is indicated by the direction of its axial magnetic field, represented by latitude angle Θ and longitude angle Φ in the GSE (Geocentric Solar Ecliptic) coordinate system O-XYZ. The satellite is assumed to cross the magnetic flux rope in the Earth-Sun direction (i.e., in the X direction), and the distance between the satellite trajectory and the cylinder axis is represented by the impact parameter P. P may take a positive or negative value as referenced to the $\vec{e_x} \times \vec{e_z}$ direction, depending on which side of the magnetic flux rope the satellite crossed. The observed solar wind velocity should then be the sum of bulk velocity of the flux rope U in the $-$X direction and the X component of expansion velocity.

In summary, eight parameters are necessary for reconstruction of the observed data according to the self-similar expanding cylindrical magnetic flux rope, consisting of: four parameters that define the shape and thickness of the magnetic flux rope (s, B_0, R_0, and t_0); three parameters that define the relative geometrical relationship between the magnetic flux rope and the satellite trajectory (Θ, Φ, and P); and the bulk velocity of the magnetic flux rope (U). The model is applied to the observation data for the magnetic field within the magnetic flux rope and the solar wind velocity, and the parameters are determined by the non-linear least-squares fitting method. It should be noted here that s can be determined simply from the direction of rotation of the observed magnetic field vector in the Y-Z plane. It can be seen that for the two types of rope structures shown in Fig.1, when a satellite enters the rope from the front and exits from the reverse side of the sheet, the observed magnetic field vector should rotate counter-clockwise for parallel type flux rope, and clockwise for anti-parallel type. Also, given seven parameters other than s, we can calculate the time it takes for the satellite to cross the magnetic flux rope. Therefore, the observed duration of the magnetic flux rope should satisfy one relational expression for those seven parameters.

Details of the least-squares fitting method are described in the Appendix. Fig.3 shows an example of this fitting. The thick solid lines drawn on the observation data are model values of the magnetic field and solar wind velocities. The vertical dashed lines represent the time at which the shock was observed. The bottom panel in Fig.3 is a plot of the magnetic field vector projected onto the X-Y, X-Z, and Y-Z planes. The figure clearly shows that the magnetic field vector rotates in the counter-clockwise direction in the Y-Z plane during the time of observation of the magnetic flux rope between the two vertical lines in the upper panels. Table 1 shows the parameters

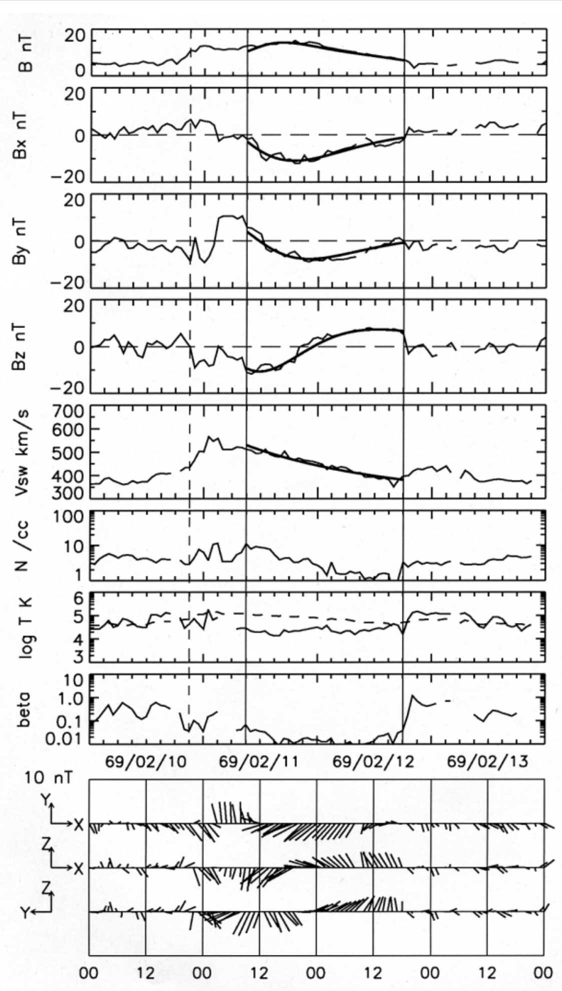

Fig.3 A result of model fitting for an interplanetary magnetic flux rope

calculated from this analysis. Fig.4 is a schematic diagram of this magnetic flux rope, displaying only the toroidal magnetic field at the surface of the cylinder. The axis is tilted approximately 11˚ southward from the ecliptic plane and directed 238˚ from the direction of the Sun. This figure depicts an expanding magnetic flux rope as it moves away from the Sun toward the Earth in the direction of the white arrow.

The satellite is moving relative to the flux rope along the X-axis, and as it passes the north side of the rope axis, it first observes a southward magnetic field. Then, as it moves on, the observed magnetic field gradually turns northward. In Fig.3, the solar wind velocity is seen to decrease from 500 km/s to 400 km/s within the magnetic flux rope. This is due to the added effect of the expansion

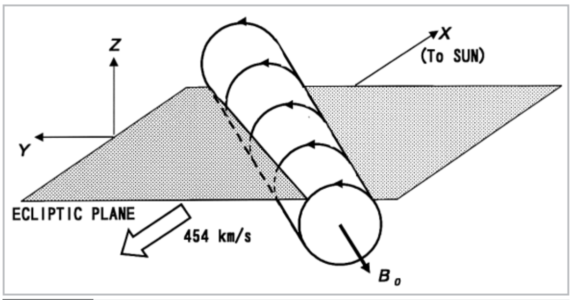

Fig.4 Schematic diagram of the magnetic flux rope configuration in Fig.3

Table 1 Parameters obtained for the magnetic flux rope in Fig.3

(Results from fitting to cylinder model)

Parameter	Value
S	1 (parallel type)
B_0	20.3 nT
R_0	0.12 AU
t_0	56 hours
Θ	−10.9 deg
Φ	238 deg
P	$-0.32R_0$
U	454 km/s

velocity of the magnetic flux rope on the bulk motion. The asymmetrical changes in the magnetic field strength can also be explained by the expansion of the magnetic flux ropes.

2.3 Interplanetary Magnetic Flux Ropes and the Solar Coronal Magnetic Fields

This section will introduce an example of analysis performed for the purpose of identifying the solar phenomena responsible for the generation of interplanetary magnetic flux ropes[10]. In this analysis, 12 cases of interplanetary magnetic flux ropes displaying smooth and large magnetic field vector rotations were selected from among those observed between 1965 and 1978. Fittings to magnetic flux rope models were performed for the selected cases to calculate the parameters of the flux rope. Next, the generation time of the magnetic flux rope on the Sun was calculated based on the velocity of the magnetic flux rope flow obtained from analysis (within

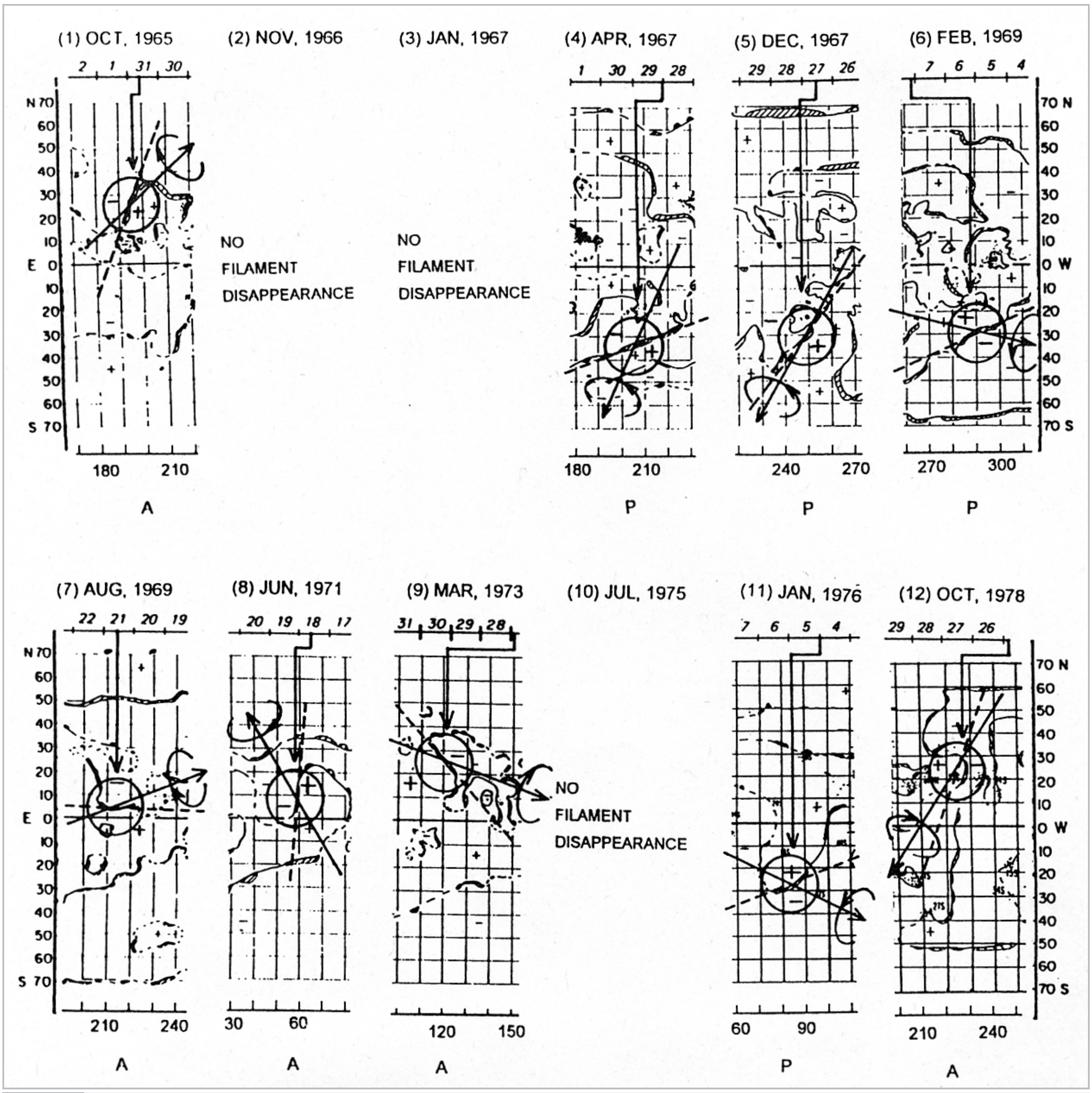

Fig.5 *Filament disappearances associated with interplanetary magnetic flux ropes*

a margin of error of ±1 day), and candidate solar activities that occurred during the determined time period were surveyed. The investigated solar activities consisted of solar flares accompanying type II/IV solar radio bursts in the meter-wave band and filament disappearances observed in the Hα line. These phenomena have conventionally been considered to have strong connections to plasma cloud generation[19][20].

Results of this analysis have shown that in nine out of the 12 cases, occurrences of filament disappearance were confirmed within a heliographic longitude range of ±30° relative to the Sun-Earth line during the estimated time period for interplanetary magnetic flux rope generation on the Sun. No correlations with solar flare occurrences were noted. Fig.5 is a representation of the relationship between interplanetary magnetic flux ropes and filament disappearances on the Sun. Filaments are formed at the boundary referred to as the neutral line at which the vertical magnetic field on the solar surface changes polarity. The filaments that disappeared are circled, and the dashed lines represent their approximate directions. The magnetic polarities on both sides of the neutral line are shown by + (outward) and

− (inward). The magnetic flux ropes are projected onto the corresponding filaments, and the directions of their axial magnetic fields are represented by long arrows. The toroidal magnetic fields on the surface of the cylinders are indicated around the tip of each such arrow. The arrows connecting the timeline at the top of each diagram to the filament show the time of filament disappearance, estimated within a margin of error of ±12 hours.

Fig. 5 reveals several features of the relationship between interplanetary magnetic flux ropes and filament disappearances.

(1) The direction of the interplanetary magnetic flux rope axis is generally aligned with the direction of the disappearing filaments.

(2) The direction of the toroidal magnetic field on the outer surface of the interplanetary magnetic flux rope coincides with the direction of the looped magnetic field produced over the neutral line in the solar corona.

(3) The axial magnetic field of the interplanetary magnetic flux rope is aligned with the neutral line and directed so that it forms with the toroidal field a parallel-type configuration for filament disappearance in the southern hemisphere and an anti-parallel configuration for that in the northern hemisphere. [The twist directions of the magnetic flux ropes are indicated below each plot with a P (parallel) or an A (anti-parallel).]

The filament disappearance discussed above is the same phenomenon as a prominence eruption. According to CME statistics drawn from observations by the SMM satellite launched in 1980, prominence eruptions are seen with higher correlation with CMEs than other CME-associated phenomena[21]. However, in some cases the SMM satellite observed no prominent solar phenomena accompanying CME. This may correspond to the three cases in Fig.5 in which no prominent solar phenomena were observed during interplanetary magnetic flux rope generation. Fig.6 shows a typical example of CME observation. As is seen in this figure, prominences are generally observed to erupt as a part of the CMEs, and CMEs generally consists of three parts: a bright frontal loop followed by a dark cavity surrounding a bright core of prominence[22]. Detailed observation of a filament reveals that the filament itself has a twisted magnetic field structure, similar to that of magnetic flux ropes, and that this structure is twisted in opposite directions in the south and north hemispheres[23][24].

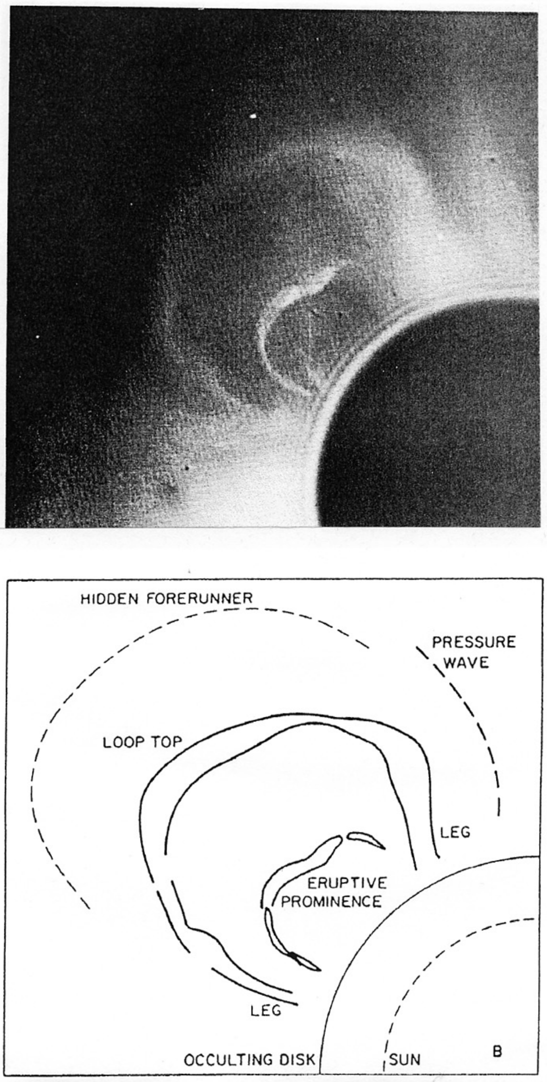

Fig.6 A typical CME observed by SMM satellite

Summarizing the above, we can propose the following scenario for the generation of an interplanetary magnetic flux rope.

"Immediately before the launch of a CME, the magnetic field in the source region overlying the filament already develops into a structure resembling a flux rope with parallel and anti-parallel twists in the southern and northern hemispheres, respectively. This structure extends and expands into interplanetary space with its orientation maintained, and is observed as an interplanetary magnetic flux rope."

A magnetohydrodynamic (MHD) simulation has shown that the CME can be generated due to an instability in the magnetic arcade structure which develops as a result of shear motion in opposite directions at two legs of the arcade[25]. The results of this simulation also support the above scenario. In this scenario, the magnetic flux rope is believed to occupy both the dark region and the prominence of the CME structure in Fig.6. Given this scenario, it should be possible to roughly predict the nature of the ejected interplanetary magnetic flux rope based on the solar magnetic field structure of the source region of the CME or the region surrounding the disappearing filament. However, in order to fully understand the difference in the directions of the disappearing filament and the corresponding interplanetary magnetic flux rope, more detailed analysis is required; this analysis will need to take into consideration the difference between the magnetic field structure in the corona and that in the chromosphere where filaments are formed and will also need to address the temporal variations during the development of CMEs[26].

Fig.7 is a schematic diagram of interplanetary magnetic flux ropes for cases of the magnetic flux rope with its axis (a) parallel to the ecliptic plane, (b) perpendicular to the ecliptic plane. Diagram (c) depicts the internal magnetic field for anti-parallel type in the rope corresponding to case (a). In this figure, the magnetic flux rope erupts with a length of 60° angular extension and propagate radially into interplanetary space, with both ends fixed on the Sun, forming a spiral pattern due to Sun's rotation. The effect of the Sun's rotation cannot be shown in (b), so a plot of projection rotated onto the meridian plane is shown.

2.4 A New Method of Analysis for Interplanetary Magnetic Flux Ropes

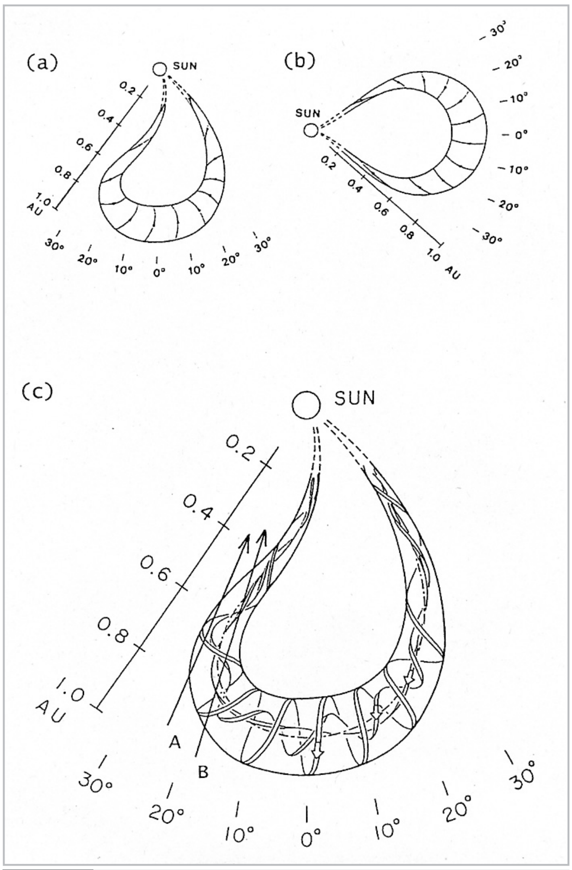

Fig.7 Schematic diagram of the entire interplanetary magnetic flux rope as it extends and expands

Analysis of the interplanetary magnetic flux rope using a cylindrical model has greatly advanced our understanding of the magnetic field structure of the plasma cloud. However, the simplified model still leaves many problems to be solved. Recently, two new approaches have been taken to develop a new method of analysis of magnetic flux ropes. The first is a modification of the curved interplanetary magnetic flux rope model[10], and the other is an analysis that takes plasma pressure into consideration[27]. These two methods are briefly described below.

If the interplanetary magnetic flux rope is assumed to have the shape shown in Fig.7, a cylindrical model can be used for interpretation of observations when a satellite passes through central parts of the rope. However, when the satellite follows the course shown by arrows A and B in Fig.7 (c), the curvature of the magnetic flux rope becomes an important element. A toroidal magnetic flux rope is a promising model to allow us to approximate the structure of the magnetic flux rope in such cases. A torus is created by bending a long cylinder. It must be noted, however, that while an exact solution is obtained for the cylindrical force-free magnetic field, an exact solution for the toroidal force free magnetic field has yet to be obtained. At present, only an approximate solution has been found, which is valid under the condition that the major radius of the torus is sufficiently larger than the minor radius[28]. Here, the model will be even more simplified and will assume that the axis of the magnetic flux rope is circular and that the internal magnetic field is defined simply as a function of distance from the axis (r) and given by Eqs. (15), (16), and (17).

Fig.8 shows an example of fitting using this model. It can be seen from the figure that this fitting produces satisfactory results. The parameters calculated by the fitting are given in Table 2. In the toroidal model, not only parameter R_0 (minor radius of torus corresponding to the thickness of the magnetic flux rope), but also parameter R_C (major radius of torus corresponding to the radius of the circle drawn by the axis of the magnetic flux rope) is needed. The overall tilt of a torus is given by Θ_n and Φ_n, the latitude and longitude angles of the normal vector of the circular plane defined by the torus axis. Parameter d indicates the direction of the X component of the axial magnetic field at X=0 on the satellite trajectory: d=1 or d=−1 for the sunward or anti-sunward direction, respectively. The impact parameters are represented by the Y-coordinate P_Y and the Z-coordinate P_Z of the satellite trajectory. Fig.9 is a schematic diagram showing the geometric configuration of the interplanetary magnetic flux rope obtained by this analysis. The parameters in Table 2 indicate that the torus is positioned in a plane tilted only 18° from the X-Z plane, and that the satellite passed far to the west of the torus along the X-axis.

It should be noted that, as seen from the vector representation in Fig.8, there is almost no change in the magnetic field while the satellite passes through the magnetic flux rope. This can be also understood from Fig.9, which shows a satellite trajectory nearly parallel to the axis of the magnetic flux rope. Clearly, such situations do not exist for linear cylindrical magnetic flux ropes. It is seen that the introduction of a toroidal magnetic flux rope model can provide a rational explanation for the previously unexplained changes in solar wind magnetic fields.

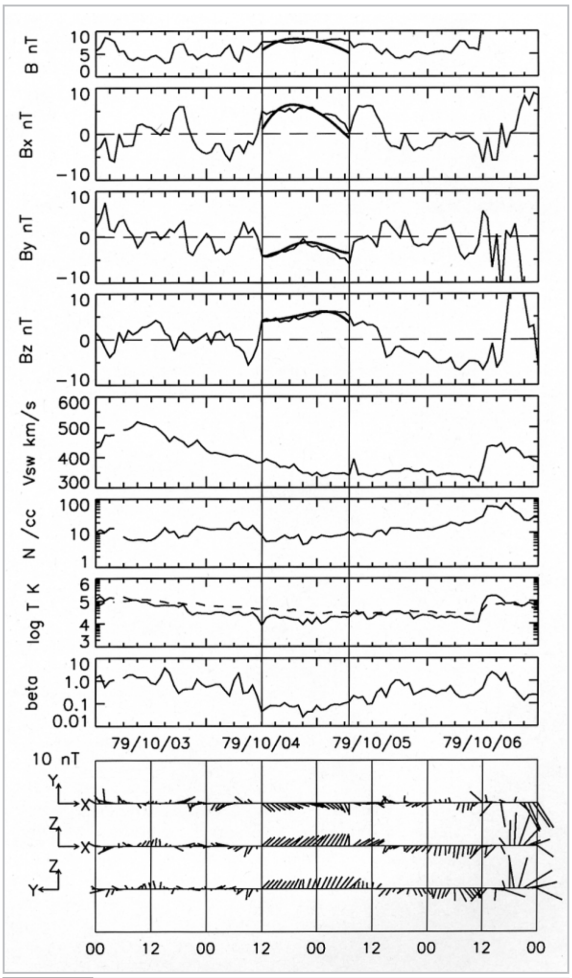

Fig.8 *Example of observation fitted to a toroidal model*

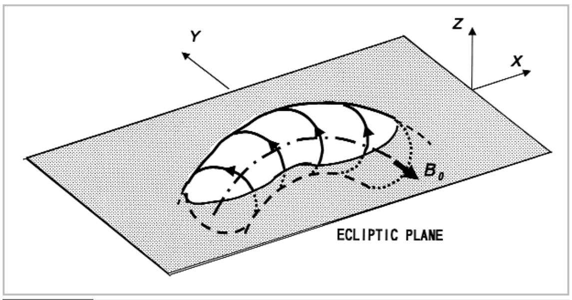

Fig.9 *Geometrical configuration of the magnetic flux rope in Fig.8*

Table 2 Parameters obtained for the magnetic flux rope in Fig.8

(Results from fitting to torus model)

Parameter	Value
s	−1 (anti-parallel type)
d	1 (Toward Sn)
B_0	11.3 nT
Rc	0.193 AU
Ro	0.025 AU
t_0	144 hours
Θn	18.1 deg
Φn	271 deg
P_Y	−0.58 Ro
P_Z	−0.14 Ro
U	359 km/s

The plasma pressure within an interplanetary magnetic flux rope is generally small compared to the magnetic field pressure, but it is not necessarily negligible. In cases where plasma pressure cannot be ignored, it will be interesting to examine how the magnetic field structure would deviate from force-free fields due to the effects of changes in plasma pressure. Recently, a method has been developed for analysis of interplanetary magnetic flux ropes that takes plasma pressure into consideration[27].

When changes in both the plasma and the magnetic field are 2-dimensional and involve no changes in the z-direction, magnetic field B can be expressed, with the orthogonal coordinate system x, y, and z referenced to that direction, as follows:

$$B = (\partial A(x,y)/\partial y,\ -\partial A(x,y)/\partial x,\ Bz) \tag{18}$$

By substituting this into Eq. (1) and from $\partial/\partial z \equiv 0$, it can be seen that plasma pressure P and B_Z both become a function of only the vector potential $A(x,y)$[29]. Eq. (1) can then be converted into:

$$\partial^2 A/\partial x^2 + \partial^2 A/\partial y^2 = -\mu_0 (d/dA)\{p(A) + [B_z(A)]^2/2\mu_0\} \tag{19}$$

If the z direction is selected appropriately, the x-axis can be defined so as to contain the satellite trajectory in the x-z plane. Then, the vector potential on the x-axis can be expressed as:

$$A(x,0) = \int_0^x (\partial A/\partial \xi) d\xi = \int_0^x -B_y(\xi,0) d\xi \tag{20}$$

Based on this equation and on the observation data, it is possible to calculate:

$$P_t(x,0) = \left[p(x,0) + B_z^2(x,0)/2\mu_0\right] \tag{21}$$

If the z-axis is appropriately selected, the plots of $A(x,0)$ versus $P_t(x,0)$ fall on the same curve for both satellite's approach and departure toward and from z-axis, because of the symmetry of plasma and field with respect to z-axis. In the actual analysis, this characteristic is used in determining the appropriate z-axis through least-squares fitting. Then, after appropriately selecting the x- and y-axes, the vector potential $A(x,y)$ and magnetic field $B_{x,y}(x,y)$ are calculated for all y values using the following equation.

$$A(x, y \pm \Delta y) \cong A(x,y) + (\partial A/\partial y)_{x,y}(\pm \Delta y) + (1/2)(\partial^2 A/\partial y^2)_{x,y}(\pm \Delta y)^2 \tag{22}$$

$$B_x(x, y \pm \Delta y) \cong B_x(x,y) + (\partial^2 A/\partial y^2)_{x,y}(\pm \Delta y) \tag{23}$$

$$B_y(x, y \pm \Delta y) \cong B_y(x,y) - (\partial^2 A/\partial x \partial y)_{x,y}(\pm \Delta y) \tag{24}$$

Fig.10 shows an example of an interplanetary magnetic flux rope obtained from this analysis. This method of analysis is extremely interesting in that it produces a magnetic field with a magnetic flux rope structure by simply assuming only a symmetrical structure for the internal magnetic field of the flux rope.

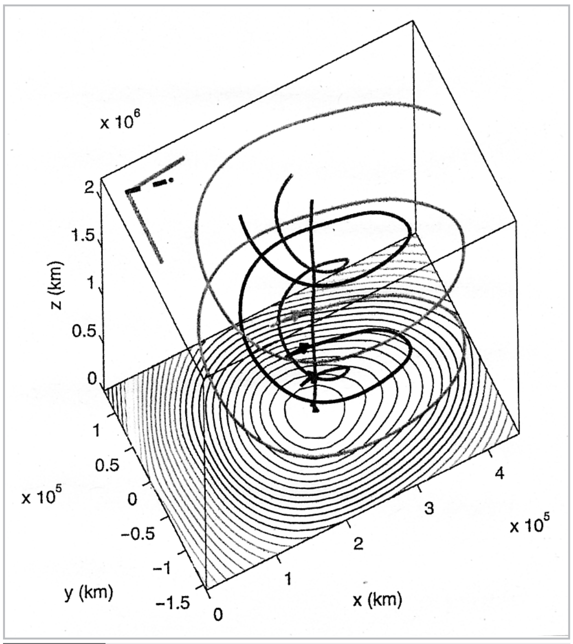

Fig.10 Example of a magnetic flux rope calculated as a function of the vector potential [28]

3 Interplanetary Magnetic Flux Ropes and Geomagnetic Storms

The role of interplanetary magnetic flux ropes in producing strong southward IMF causing geomagnetic storms was reexamined[7] for 10 geomagnetic storms with recorded *Dst* of -100 or below between 1978 and 1979[30] and for the five largest geomagnetic storms from 1971 to 1986[31]. The results confirmed the presence of an interplanetary magnetic flux rope in most cases. To illustrate one particularly significant example, presented below are the results for a geomagnetic storm that took place on Nov. 25, 1978.

Fig.11 shows the changes observed in the IMF, solar wind plasma, and *Dst* during four days including the geomagnetic storm period. The SC indicating the sudden commencement of a geomagnetic storm was observed at 12:22 UT. The dashed line shows the time at which the corresponding solar wind shock was observed. Based on the changes in solar wind around the shock, it is concluded that this shock was a co-rotational shock formed by high-speed solar winds, being steadily ejected from a coronal hole, with a velocity reaching 600 km/s on Nov. 26[32]. The thick, horizontal bar displayed at the top of the figure indicates the period during which bi-directional hot electron flux was confirmed[5]. The dashed line in the plot of proton temperature *T* shows the changes in proton temperature statistically expected from solar wind velocity[33]. It can be seen that abnormally low proton temperatures are observed in the time interval between the first solid line and the time of shock[6]. As discussed in Section 1, this can be considered as proof of the presence of a plasma cloud having originated from CME. Based on the changes in the solar wind velocity V_{SW}, density *N*, and proton temperature *T*, it is concluded that the plasma cloud encountered the high-speed flow at the time designated by the second solid line.

It is thus reasonable to conclude that an interplanetary magnetic flux rope occupies the time period between the two solid lines, and that the magnetic field is strongly deformed by the shock after the time indicated by the dashed line. The smooth solid lines drawn between the two solid lines represent the results of fitting to a cylindrical magnetic flux rope model based on the above interpretation. Table 3 shows the calculated parameters.

The following conclusions can be drawn from this analysis. The strong southward IMF that caused this geomagnetic storm is the southward magnetic field in the rear portion of the interplanetary magnetic flux rope; this field has been intensified by the shock formed by the high-speed solar wind that has overtaken the flux rope. It can be seen from Table 3 that the satellite traversed the magnetic flux rope through the portion significantly distant from the axis, resulting in only a small rotation of the observed magnetic field vector in the Y-Z plane. This is why the magnetic field change in this event had not been attributed to magnetic flux rope in conventional analysis.

Fig.12 is a sketch of the possible shape of the above interplanetary magnetic flux rope, and it also shows the location of a filament disappearance corresponding to its generation. According to the records of the Paris Observa-

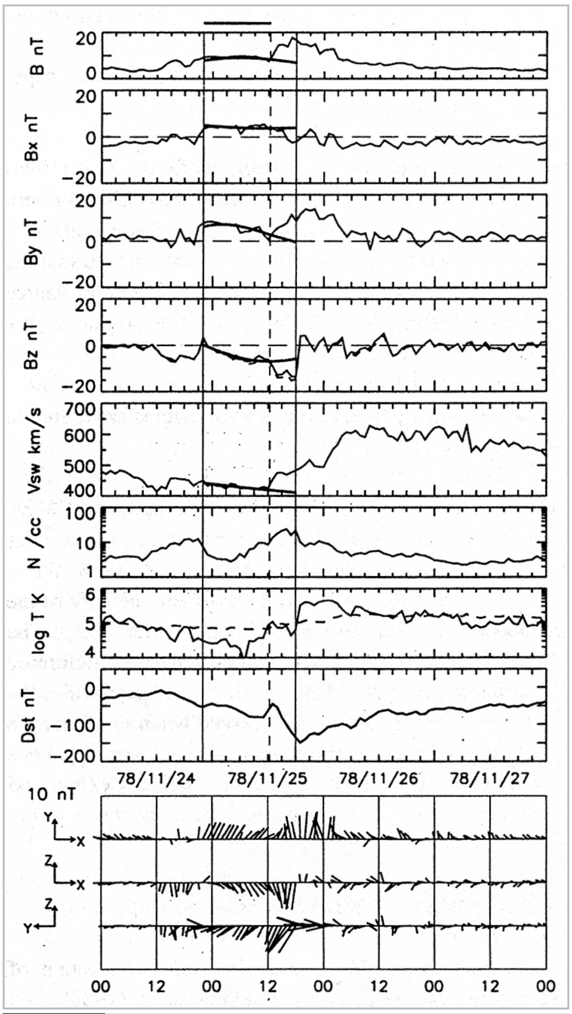

Fig. 11 *Geomagnetic storm on Nov. 25, 1978 and the corresponding changes in solar wind*

Table 3 *Parameters obtained for the magnetic flux rope in Fig. 11*

(Results from fitting to cylinder model)

Parameter	Value
s	1 (parallel tyoe)
B_0	15.4 nT
R_0	0.12 AU
t_0	141 hours
Θ	−29 deg
Φ	140 deg
P	0.85 R_0
U	427 km/s

tory, the filament circled in the southern hemisphere was observed on Nov. 19 and had already disappeared on Nov. 20. This means that at least four days and 12 hours had passed from the time of filament disappearance to the observation of the magnetic flux rope near Earth. Since the average velocity of the interplanetary magnetic flux rope is 427 km/s, its leading edge should reach the Earth's orbit 97 hours after the filament disappearance. Therefore, a possible interpretation for the storm occurrence is given as follows. A parallel-type magnetic flux rope as observed by the satellite was generated in association with the filament disappearance in the southern hemisphere. This is consistent with the general relationship between flux ropes and filament disappearances as described in Section 2.3. Then, the flux rope extended into interplanetary space with the direction of its axis maintained generally parallel to the filament direction. It is not until the central part (the loop top) of the flux rope reached a point beyond the Earth's orbit that the western leg of the magnetic flux rope brushed past the Earth.

The results of this analysis have several implications for future studies of the interplanetary magnetic flux rope. The first is that even for small IMF rotation angles, contact with a solar magnetic flux rope can in some cases be confirmed. In other words, many cases of encounter with magnetic flux ropes could be overlooked if only large rotation angles are used as a criterion for identification of magnetic flux ropes. The second implication is a caution needed when comparing the direction of the interplanetary magnetic flux rope detected near Earth and the direction of the flux rope immediately after its generation in the CME. As a prerequisite for such comparisons, the portion of the interplanetary magnetic flux rope observed by the satellite must be correctly defined relative to the entire magnetic flux rope. Finally, it must be noted that the leg of an interplanetary magnetic flux rope generated on the east side of the Sun-Earth line continues to exist near Earth long after the top portion has passed the Earth's orbit, and that this leg may be observable from Earth.

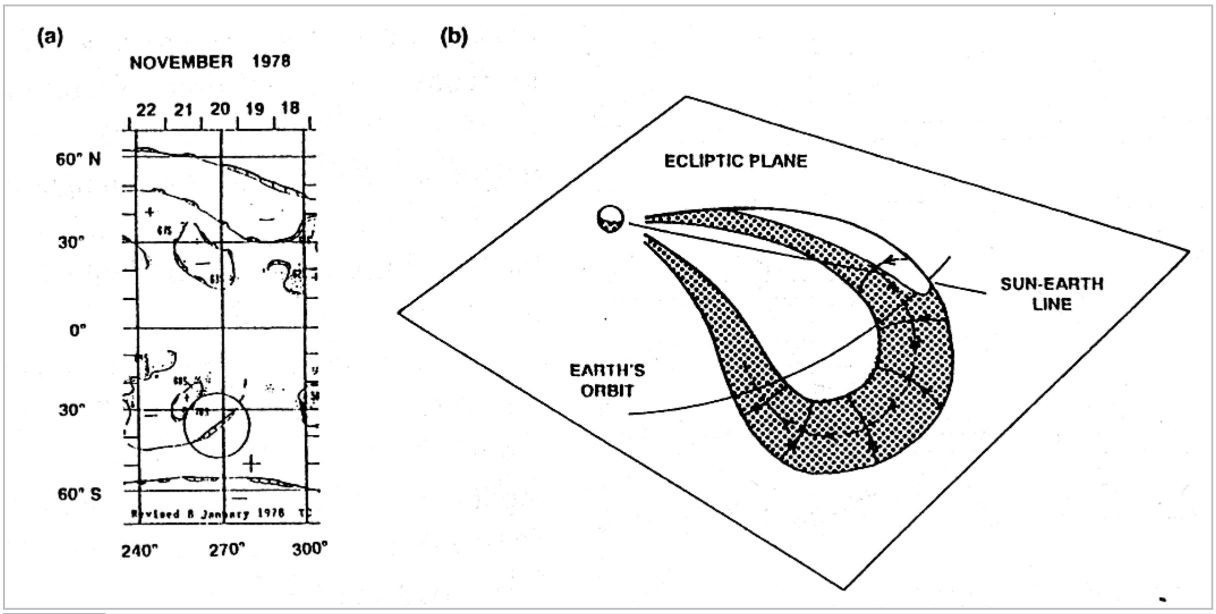

Fig. 12 The shape of the magnetic flux rope observed on Nov. 25 and the corresponding filament disappearance

4 Themes of Future Research

The study of the interplanetary magnetic flux rope began with an analysis of the solar wind. Comparison of the obtained magnetic flux rope structure with associated solar phenomena has led to studies of physical connection between magnetic flux ropes and CMEs. For further understanding of the generation of the interplanetary magnetic flux ropes in the solar corona and their propagation into the Earth's orbit, many problems still remain to be solved both in analyzing solar wind data and in relating the magnetic flux rope to CMEs.

We discuss three problems in establishing a method to determine the occurrence of interplanetary magnetic ropes based on solar wind observations and in the subsequent analysis to determine their geometry. The first problem is the difficulty encountered in determining a magnetic flux rope structure from solar wind data. Attempts have been made to develop methods for the automatic detection of magnetic flux ropes from solar wind data based on the smoothness of changes in the magnetic field within the magnetic flux rope[34]. However, more detailed algorithms must be developed to realize a completely automatic detection system. Furthermore, even when a magnetic flux rope can be successfully identified, the problem of locating its boundaries remains, particularly in the case of the rear boundary. The determination of the boundary significantly affects the subsequent calculation of the geometrical parameters of the magnetic flux rope. Theoretically, the boundary of a magnetic flux rope is considered to be a discontinuity formed at the contact surface of two plasma regimes from different sources. It would be useful to develop an effective algorithm that allows us to detect weak discontinuities in data with high temporal resolution.

The second, and more important, problem is the strong model-dependency of the geometrical parameters of a magnetic flux rope determined by the least-squares fitting method. The force-free field with constant α is one extreme model to describe magnetic flux rope structures. There is no guarantee that this model is consistent with the actual state of the magnetic flux rope structure. The direction of the axis determined by the least-squares fitting method changes depending on how the magnetic field strength of the cylindrical magnetic flux rope varies in the radial direction. Accordingly, we may get valuable insights by evaluating the consistency between the magnetic field distribution determined from analysis without assuming a magnetic field structure[27] and that determined from analysis assuming a force-free field with constant α. Also, a precise numerical formula must be derived for a magnetic flux rope with a thick torus shape (with the major radius, at most, only several times larger than the minor radius). It must be noted that there are cases in which the changes in the magnetic field of a single magnetic flux rope can be explained equally well by either the cylindrical or the toroidal model. In such cases, it should be possible to judge which model is more appropriate by determining the direction of discontinuity surface at the boundary.

Finally, there is the problem of the global configuration of interplanetary magnetic flux rope in interplanetary space. The schematic diagram in Fig.7 represents an imagined structure by summarizing analysis results for many observed magnetic flux ropes. At present, only the results of MHD simulations provide information on the way how and which part of the CME as shown in Fig.6 extends into the solar wind. Currently, 3-D simulations applied to the combined system of the solar corona and the solar wind are only in the initial stages[35]. Given these conditions, it seems promising to make observations of a single interplanetary magnetic rope at different positions using multiple satellites[36]. Detailed analysis of such data should provide valuable information not only on the global configuration of the magnetic flux rope in interplanetary space but also on the distribution of the internal magnetic field.

We consider also three problems regarding the physical connection between the interplanetary magnetic flux rope and the CME. The first is a problem encountered when determining the source region and the generation time of the observed interplanetary magnetic flux rope on the solar surface or in the corona. CMEs occurring near the center of the solar disk that are capable of ejecting magnetic flux ropes toward Earth are called halo CMEs, and are generally difficult to detect. It is possible to estimate the time and source region of CME generation when soft X-ray LDEs (Long Duration Events)[37], EIT waves (as observed by the SOHO satellite)[38] and filament eruptions occur simultaneously with CMEs. However, there are cases in which no remarkable solar activities are observed even when a CME has occurred. Furthermore, even when the above CME-associated phenomena are observed, only indirect evidence links them to interplanetary magnetic flux rope generation, such as temporal relationships and similarities in the magnetic field. Although this problem is extremely difficult to resolve, it should become less intractable as improvements are made in the sensitivity of observation instruments. A peculiar state of ion composition has been detected by the latest Solar Wind Ion Composition Spectrometer (SWICS) onboard the ACE satellite, in which the ion composition within a magnetic flux rope consists of a mixture of ions produced at low temperatures ($\leq 0.2 \times 10^6$ K) and those produced at higher temperatures (4×10^6 K)[39]. By comparing the analysis of this data with a detailed analysis of the solar corona, it should be possible to determine the coronal region in which the magnetic flux rope originated. Such analysis is providing new information linking the interplanetary magnetic flux rope to its source region in the solar corona.

The second problem is concerned with the relationship between the direction of the interplanetary magnetic flux rope and the direction of the neutral line of the solar surface magnetic field estimated from the corresponding filament. As seen in Fig.5, the two are irregularly offset from each other. The soft X-ray telescope (SXT) onboard the Yohkoh satellite has observed magnetic arcade structures after CME launch in numerous cases. It has been reported that the coronal magnetic fields inferred from such arcade structures generally are much more simplified than the solar surface magnetic field, and that the arcades are observed to extend along the neutral lines rather than along the filaments[40]. The arcade magnetic field structure is believed to be the trace formed after the ejection of magnetic flux rope, and so the direction of its extension on the solar surface and the direction of the ejected magnetic flux rope are expected to roughly coincide. It has also been pointed out that, in interplanetary space, the plane along which the interplanetary magnetic flux rope lies does not coincide with the heliospheric neutral sheet determined from the spatial distribution of IMF[41]. The relationship between the magnetic neutral line on the solar surface, the arcade structure observed via soft X-ray, the interplanetary magnetic flux rope, and the IMF neutral sheet is a challenging theme of MHD simulation studies; however this theme can undoubtedly be clarified through detailed analysis of the observational data.

Finally, there is a problem regarding the deformation and changes in velocity of the magnetic flux rope during its ejection from the solar corona and its propagation through interplanetary space. The deformation of the magnetic flux rope must be taken into consideration when comparing the results of solar wind observation and CME source region observation. With advancements in MHD simulation, it should eventually be possible to evaluate the effect of such deformation correctly. At present, however, this can only be evaluated through comparison of data for a single magnetic flux rope observed at different distances from the Sun using multiple spacecraft. The change in velocity during propagation must be taken into account when estimating the time at which an interplanetary magnetic flux rope observed near Earth was ejected from the Sun. One study has presented a statistical evaluation of the acceleration and deceleration of interplanetary magnetic flux ropes based on a comparison of the CME velocity observed by the Solwind and SMM satellites and the interplanetary magnetic flux rope velocity observed by the Pioneer Venus Orbiter (PVO) and by the Helios satellite[42].

Below are themes for future studies that will be important in clarifying the relationship between the interplanetary magnetic flux rope structure and CME.

(1) Development of an algorithm to detect various changes in IMF related to interplanetary magnetic flux ropes
(2) Analysis of the discontinuity at the boundary of a magnetic flux rope and analysis of the interaction between the magnetic flux rope and the background solar wind
(3) Comparison of analyses that employ different models of interplanetary magnetic flux ropes
(4) Derivation of a numerical formula describing a thick toroidal magnetic flux rope
(5) Analysis of data from multiple-satellite observation of a single interplanetary magnetic flux rope
(6) Analysis of ion composition and charge state within the magnetic flux rope
(7) Comparison of the soft X-ray arcade structure created at the CME source region and the interplanetary magnetic flux rope
(8) A 3-D MHD simulation connecting the solar corona and the solar wind

5 Conclusions

Strong southward IMFs triggering the development of large geomagnetic storms are frequently transported from the Sun by interplanetary magnetic flux ropes. It can be concluded based on the results of foregoing studies that the interplanetary magnetic flux rope is ejected from the solar corona during the course of a CME and that it extends riding on the solar wind with the original magnetic field structure preserved. Given these conclusions, it seems possible in the near future to determine the characteristics of an ejected magnetic flux rope based on observations of magnetic field structures of the CME source region on the Sun and to develop a method to apply this information to geomagnetic storm prediction. This paper has provided an introduction to the research that has led to the above conclusions and has examined some themes for future studies that may contribute to progress in this area.

Acknowledgements

The author is grateful to former Distinguished Researcher Dr. Takashi TANAKA and Senior Researcher Mr. Hirotaka MORI of the CRL for their guidance in the development of the non-linear least-squares fitting program used in this paper.

References

1 T. Ondoh and K. Marubashi, Science of Space Environment, Ohmusha, Tokyo, 2001.

2 B.T. Tsurutani and W.D. Gonzalez, "The interplanetary causes of magnetic storms: A review", in Magnetic Storms, Geophys. Monogr. Ser., Vol. 98, edited by B.T. Tsurutani, W.D. Gonzalez, Y. Kamide, and J.F. Arballo, AGU, Washington, D.C., pp. 77-89, 1997.

3 J.T. Gosling, "Coronal mass ejections and magnetic flux ropes in interplanetary space", in Physics of Magnetic Flux Ropes, Geophys. Monogr. Ser., Vol. 58, edited by C.T. Russell, E.R. Priest, and L.C. Lee, AGU, Washington, D.C., pp. 330-364, 1990.

4 M. Neugebauer and R. Goldstein, "Particle and field signatures of coronal mass ejections in the solar wind", in Corona Mass Ejections, Geophys. Monogr. Ser., Vol. 99, edited by N.U.Croker, J.A. Joselyn, and J. Feynman, AGU, Washington, D.C., pp. 245-252, 1997.

5 J.T. Gosling, D.N. Baker, S.J. Bame, W.C. Feldman, R.D. Zwickl, and E.J. Smith, "Bidirectional solar wind electron heat flux events", J. Geophys. Res., Vol. 92, pp. 8519-8535, 1987.

6 I.G. Richardson and H.V. Cane, "Regions of abnormally low proton temperature in the solar wind", J. Geophys. Res., Vol. 100, pp. 23,397-23,412, 1995.

7 K. Marubashi, "Physics of interplanetary magnetic flux ropes: Toward prediction of geomagnetic storms", Adv. Space Res. Vol. 26, no. 1, pp. 55-66, 2000.

8 W.D. Gonzalez, J.A. Joselyn, Y. Kamide, H.W. Kroehl, G. Rostoker, B.T. Tsurutani, and V.M. Vasyliunas, "What is a geomagnetic storm?", J. Geophys. Res., Vol. 99, pp. 5771-5792, 1994.

9 K. Marubashi, "Structure of the interplanetary magnetic clouds and their solar origins", Adv. Space Res. Vol. 6, no. 6, pp. 335-338, 1986.

10 K. Marubashi, "Interplanetary magnetic flux ropes and solar filaments", in Corona Mass Ejections, Geophys. Monogr. Ser., Vol. 99, edited by N.U.Croker, J.A. Joselyn, and J. Feynman, AGU, Washington, D.C., pp. 147-156, 1997.

11 V. Bothmer and R. Schwenn, "Eruptive prominences as sources of magnetic clouds in the solar wind", Space Sci. Rev., Vol. 70, pp. 215-220, 1994.

12 V. Bothmer and R. Schwenn, "The structure and origin of magnetic clouds in the solar wind", Ann. Geophys., Vol. 16, pp. 1-24, 1998.

13 H. Alfvén and C.-G. Fälthammer, Cosmical Electrodynamics, Oxford Press, 1963.

14 L.F. Burlaga, E. Sittler, F. Mariani, and R. Schwenn, "Magnetic loop behind an interplanetary shock: Voyager, Helios, and IMP 8 observations", J. Geophys. Res., Vol. 86, pp. 6673-6684, 1981.

15 H. Goldstein, "On the field configuration in magnetic clouds", in Solar Wind Five, NASA Conf. Publ., No. 2280, pp. 731-733, 1983.

16 L.F. Burlaga, "Magnetic clouds and force-free fields with constant alpha", J. Geophys. Res., Vol. 93, pp. 7217-7224, 1988.

17 C.J. Farrugia, L.F. Burlaga, V.A. Oshrovich, I.G. Richardson, M.P. Freeman, R.P. Lepping, and A.J. Lazarus, "A study of an expanding interplanetary magnetic cloud and its interaction with the Earth's magnetosphere", J. Geophys. Res., Vol. 98, pp. 7621-7632, 1993.

18 R.P. Lepping, J.A. Jones, and L.F. Burlaga, "Magnetic field structure of interplanetary magnetic cloud", J. Geophys. Res., Vol. 95, pp. 11,957-11,965, 1990.

19 F.E. Cook and C.G. McCue, "Solar-terrestrial relations and short-term ionospheric forecasting", Radio Electronic Engineer, Vol. 45, pp. 11-30, 1979.

20 J.A. Joselyn and P.S. McIntosh, "Disappearing solar filaments: A useful predictor of geomagnetic activity", J. Geophys. Res., Vol. 86, pp. 4555-4564, 1981.

21 D.F. Webb and A.J. Hundhausen, "Activity associated with the solar origin ofcoronal mass ejections", Solar Phys., Vol. 108, pp. 383-401, 1987.

22 R.M.E. Illing and A.J. Hundhausen, "Disruption of a coronal streamer by an eruptive prominence and coronal mass ejection", J. Geophys. Res., Vol. 91, pp. 10,951-10,960, 1986.

23 J.L. Leroy, V. Bommier, and S. Sahal-Bréchot, "New data on the magnetic structure of quiescent prominences", Astron. Astrophys., Vol. 131, pp. 33-44, 1984.

24 S.F. Martin, R. Bilimoria, and P.W. Tracadas, "Magnetic field configurations basic to filament channels and filaments", in Solar Surface Magnetism, edited by R.J. Rutten and C.J. Schrijver, NATO ASI Series C, Vol. 433, Kluwer Academic Publ., Dordrecht, pp. 303-338, 1994.

25 Z. Mikic, D.C. Barnes, and D.D. Schnack, "Dynamical evolution of a solar coronal magnetic field arcade", Astrophys. J., Vol. 328, pp. 830-847, 1988.

26 D.F. Webb, R.P. Lepping, L.F. Burlaga, C.E. DeForest, D.E. Larson, S.F. Martin, S.P. Plunkett, and D.M. Rust, "The origin and development of the May 1997 magnetic cloud", J. Geophys. Res., Vol. 105, pp. 27,251-27,259, 2000.

27 Q. Hu and B.U.Ö. Sonnerup, "Reconstruction of magnetic flux ropes in the solar wind", Geophys. Res. Lett., Vol. 28, pp. 467-470, 2001.

28 G. Miller and L. Turner, "Force free equilibria in toroidal geometry", Phys. Fluids, Vol. 24, pp. 363-365, 1984.

29 P. Sturrock, Plasma Physics, An Introduction to the Theory of Astronomical, Geophysical and Laboratory Plasma, Cambridge Univ. Press, New York, p. 209, 1994.

30 B.T. Tsurutani, W.D. Gonzalez, F. Tang, S.I. Akasofu, and E.J. Smith, "Origin of interplanetary southward magnetic fields responsible for major magnetic storms near solar maximum (1978-1979)", J. Geophys. Res., Vol. 93, pp. 8519-8531, 1988.

31 B.T. Tsurutani, W.D. Gonzalez, F. Tang, and Y.T. Lee, "Great magnetic storms", Geophys. Res. Lett., Vol. 19, pp. 73-76, 1992.

32 H.V. Cane and I.G. Richardson, "What caused the large geomagnetic storm of November 1978?", J. Geophys. Res., Vol. 102, pp. 17,445-17,449, 1997.

33 R. Lopez, "Solar cycle invariance in solar wind proton temperature relationships", J. Geophys. Res., Vol. 92, pp. 11,189-11,194, 1987.

34 H. Shimazu and K. Marubashi, "New method for detecting interplanetary flux ropes", J. Geophys. Res., Vol. 105, pp. 2365-2373, 2000.

35 J.A. Linker and Z. Mikic, "Extending coronal models to Earth orbit", in Corona Mass Ejections, Geophys. Monogr. Ser., Vol. 99, edited by N.U.Croker, J.A. Joselyn, and J. Feynman, AGU, Washington, D.C., pp. 269-277, 1997.

36 T. Mulligan, C.T. Russell, B.J. Anderson, D.A. Lohr, D. Rust, B.A. Toth, L.J. Zanetti, M.H. Acuna, R.P. Lepping, and J.T. Gosling, Intercomparison of NEAR and Wind interplanetary coronal mass ejection observations, J. Geophys. Res., Vol. 104, pp. 28,217-28,223, 1999.

37 S.W. Kahler, "The morphological and statistical properties of solar X-ray events with long decay times, Astrophys. J., Vol. 214, pp. 891-897, 1977.

38 B.J. Thompson, J.B. Gurman, W.M. Newmark, J.S. Delaboudinier, O.C. St Syr, S. Stezelberger, K. P. Dere, R.A. Howard, and D.J. Michels, "SOHO/EIT observations of the 1997 April 7 coronal transient: Possible evidence of coronal Morton waves", Astrophys. J., Vol. 517, L151-L154, 1999.

39 G. Gloeckler, L.A. Fisk, S. Hefti, N.A. Schwardron, T.H. Zurbuchen, F.M. Ipavich, J. Geiss, P. Bochsler, and R.F. Wimmer-Schweingruber, "Unusual composition of the solar wind in the 2-3 May 1998 CME observed with SWICS on ACE", Geophys. Res. Lett., Vol. 26, pp. 157-160, 1999.

40 S. Watari, T. Detman and J.A. Joselyn, "A large arcade along the inversion line observed on May 19, 1992 by Yohkoh and enhancement of interplanetary energetic particles", Solar Phys., Vol. 169, pp. 167-179, 1996.

41 N.U. Crooker, J.T. Gosling, and S.W. Kahler, "Magnetic clouds and sector boundaries", J. Geophys. Res., Vol. 103, pp. 301-306, 1998.

42 G.M. Lindsay, J.G. Luhmann, C.T. Russell, and J.T. Gosling, "Relationships between coronal mass ejection speeds from coronagraph images and interplanetary characteristics of associated interplanetary coronal mass ejections", J. Geophys. Res., Vol. 104, pp. 12,515-12,523, 1999.

Appendix

A fitting of data to the interplanetary magnetic flux rope model is performed for solar wind velocity and the three components of the magnetic field observed within the magnetic flux rope. The N observation data for fitting are represented by an N-dimensional vector $\boldsymbol{Y}_0$. The corresponding values calculated from the model using M parameters $X_1, \ldots\ldots, X_M$ can be represented by an N-dimensional vector $\boldsymbol{Y}$ using function $\boldsymbol{F}$ as follows:

$$\boldsymbol{Y} = \boldsymbol{F}(X_1, \ldots\ldots, X_M) \tag{A 1}$$

or, when $X_1, \ldots\ldots, X_M$ is represented by an M-dimensional vector $\boldsymbol{Z} = \boldsymbol{Z}(X_1, \ldots\ldots, X_M)$, as:

$$\boldsymbol{Y} = \boldsymbol{F}(\boldsymbol{Z}) \tag{A 2}$$

The goal of the fitting is to determine parameters $X_1^{(m)}, \ldots\ldots, X_M^{(m)}$ that minimize $|\boldsymbol{Y} - \boldsymbol{Y}_0|$.

Suppose that parameters $X_1^{(k)}, \ldots\ldots, X_M^{(k)}$ that are near the final results are tentatively given, the corresponding vector $\boldsymbol{Y}^{(k)}$ can be approximated as follows:

$$\boldsymbol{Y}^{(k)} = \boldsymbol{Y}^{(m)} + \Sigma(\partial \boldsymbol{F}(\boldsymbol{Z}^{(k)}) / \partial X_i^{(k)}) (X_i^{(m)} - X_i^{(k)}) \tag{A 3}$$

Let $\boldsymbol{R}$ be the difference between $\boldsymbol{Y}^{(k)}$ and $\boldsymbol{Y}_0$, then

$$\boldsymbol{R} = \boldsymbol{Y}^{(k)} - \boldsymbol{Y}_0 = \boldsymbol{Y}^{(m)} - \boldsymbol{Y}_0 + \Sigma(\partial \boldsymbol{F}(\boldsymbol{Z}^{(k)}) / \partial X_i^{(k)}) \cdot (X_i^{(m)} - X_i^{(k)}) \tag{A 4}$$

If we use $\boldsymbol{P}_i$ to express the change in $\boldsymbol{Y}$ when only the i th parameter of $X_1^{(k)}, \ldots\ldots, X_M^{(k)}$ is changed, ΔX_i, then

$$\boldsymbol{P}_i = \boldsymbol{F}(X_1^{(k)}, \ldots, X_i^{(k)} + \Delta X_i, \ldots, X_M^{(k)}) - \boldsymbol{F}(\boldsymbol{Z}^{(k)}) = (\partial \boldsymbol{F}(\boldsymbol{Z}^{(k)}) / \partial X_i^{(k)}) \Delta X_i \tag{A 5}$$

By substituting (A5) into (A4), we obtain:

$$\boldsymbol{R} = \boldsymbol{Y}^{(m)} - \boldsymbol{Y}_0 + \Sigma\{(X_i^{(m)} - X_i^{(k)}) / \Delta X_i\} \boldsymbol{P}_i \tag{A 6}$$

$\boldsymbol{Y}^{(m)} - \boldsymbol{Y}_0$ approaches 0 as $\boldsymbol{Z}^{(k)}$ approaches $\boldsymbol{Z}^{(m)}$. Therefore, neglecting this part, we write $\boldsymbol{R}$ as a linear combination of $\boldsymbol{P}_i$:

$$\boldsymbol{R} = \Sigma x_i \boldsymbol{P}_i \tag{A 7}$$

$$x_i = (X_i^{(m)} - X_i^{(k)}) / \Delta X_i \tag{A 8}$$

$$\therefore \quad X_i^{(m)} = X_i^{(k)} + x_i \Delta X_i \tag{A 9}$$

Note here that:

This is a correction equation for $X_i^{(k)}$ to approach $X_i^{(m)}$.

On the other hand, when M vectors $\boldsymbol{P}_i$ are converted into M normalized orthogonal vectors $\boldsymbol{Q}_i$, the residual vector $\boldsymbol{R}$ can be expressed in a sense of the least-squares method as follows:

$$\boldsymbol{R} = \Sigma s_i \boldsymbol{Q}_i \qquad (A10)$$

$$s_i = (\boldsymbol{R}. \boldsymbol{Q}_i) \qquad (A11)$$

The conversion from $\boldsymbol{P}_i$ to $\boldsymbol{Q}_i$ is performed by first normalizing $\boldsymbol{P}_1$ into $\boldsymbol{Q}_1$, then subtracting the component parallel to $\boldsymbol{Q}_1$ from $\boldsymbol{P}_2$ before normalizing it into $\boldsymbol{Q}_2$, and so on. This successive calculation can be written as:

$$\boldsymbol{P}_i = \Sigma a_{ij} \boldsymbol{Q}_j \ (i \geqq j) \qquad (A12)$$

$$a_{11} = \sqrt{(\boldsymbol{P}_i . \boldsymbol{P}_1)} \qquad (A13)$$

$$\boldsymbol{Q}_1 = \boldsymbol{P}_1 / a_{11} \qquad (A14)$$

$$\cdots\cdots$$

$$a_{i+1\, j} = (\boldsymbol{P}_{i+1} . \boldsymbol{Q}_j) \quad (i \geqq j) \qquad (A15)$$

$$a_{i+1\, i+1} = \sqrt{\{(\boldsymbol{P}_{i+1} - \Sigma a_{i+1\, j} \boldsymbol{Q}_j).(\boldsymbol{P}_{i+1} - \Sigma a_{i+1\, j} \boldsymbol{Q}_j)\}} \qquad (A16)$$

$$\boldsymbol{Q}_{i+1} = (\boldsymbol{P}_{i+1} - \Sigma a_{i+1\, j} \boldsymbol{Q}_j) / a_{i+1\, i+1} \qquad (A17)$$

By substituting Eq. (A12) into Eq. (A7) and by comparing the coefficient of $\boldsymbol{Q}_i$ with (A10), we obtain:

$$s_i = \Sigma x_j a_{ji} \quad (j \geqq i) \qquad (A18)$$

By solving this for $\boldsymbol{x}_j$, we obtain:

$$x_M = s_M / a_{MM} \qquad (A19)$$

$$x_{M-i} = (s_{M-i} - \Sigma x_j a_{j\, M-i}) / a_{M-i\, M-i} \quad (j > M - i) \qquad (A20)$$

With these x_i ($I = 1, ..., M$) and Eq. (A9), the parameter correction is repeated using the following equation, until the values converge.

$$X_i^{(k+1)} = X_i^{(k)} + f x_i \Delta X_i \quad (I = 1, \ldots, M) \qquad (A21)$$

Here, $\boldsymbol{f}$ is the feedback factor incorporated to stabilize the calculation; it is appropriately selected from the range $0 < \boldsymbol{f} < 1$. The criteria for convergence is:

$$|\Sigma s_i \boldsymbol{Q}_i| \leqq \varepsilon \quad (\varepsilon = 10^{-5}) \qquad (A22)$$

The calculation process is outlined in the flowchart in Fig. A1.

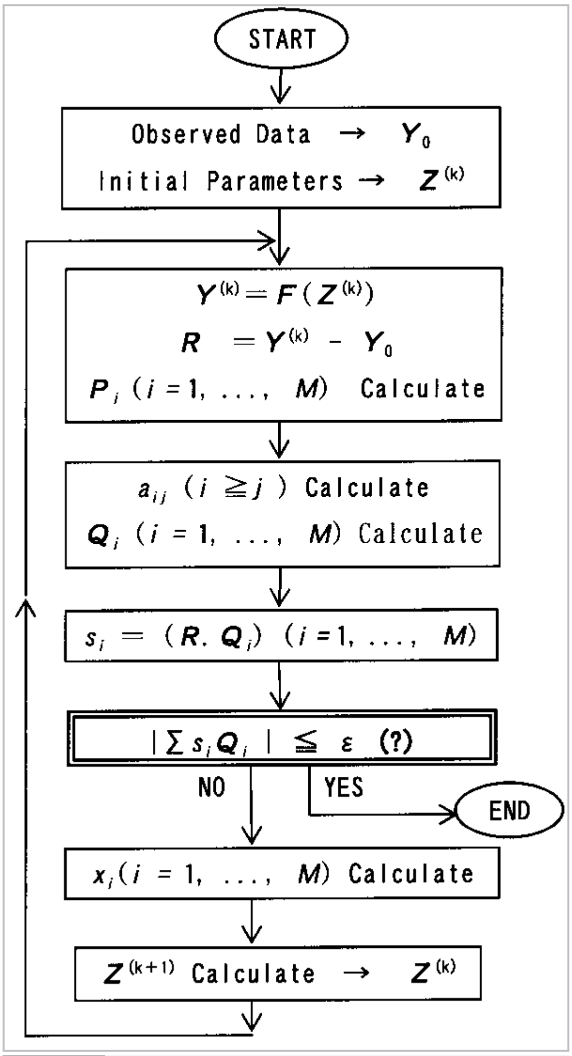

Fig.A1 *Process of calculating the most suitable parameters using the non-linear least-squares fitting method*

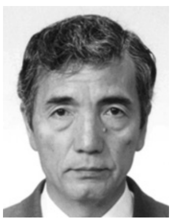

***MARUBASHI Katsuhide**, Ph. D.*

Visiting Researcher, Solar and Solar Wind Group, Applied Research and standards Division

Solar-Terrestrial Physics